Structural modifications and corrosion behavior of martensitic stainless steel nitrided by plasma immersion ion implantation

C. A. Figueroa[a)]
Australian Nuclear Science and Technology Organisation, Private Mail Bag 1, Menai, NSW 2234, Australia and Instituto de Física "Gleb Wataghin", Unicamp, 13083-970 Campinas, SP, Brazil

F. Alvarez
Instituto de Física "Gleb Wataghin", Unicamp, 13083-970 Campinas, SP, Brazil

Z. Zhang, G. A. Collins, and K. T. Short
Australian Nuclear Science and Technology Organisation, Private Mail Bag 1, Menai, NSW 2234, Australia

(Received 28 October 2004; accepted 18 April 2005; published 21 June 2005)

In this work we report a study of the structural modifications and corrosion behavior of martensitic stainless steels (MSS) nitrided by plasma immersion ion implantation (PI^3). The samples were characterized by x-ray diffraction, scanning electron microscopy, energy dispersive x-ray spectroscopy, photoemission electron spectroscopy, and potentiodynamic electrochemical measurements. Depending on the PI^3 treatment temperature, three different material property trends are observed. At lower implantation temperatures (e.g., 360 °C), the material corrosion resistance is improved and a compact phase of ε-$(Fe,Cr)_3N$, without changes in the crystal morphology, is obtained. At intermediate temperatures (e.g., 430 °C), CrN precipitates form principally at grain boundaries, leading to a degradation in the corrosion resistance compared to the original MSS material. At higher temperatures (e.g., 500 °C), the relatively great mobility of the nitrogen and chromium in the matrix induced random precipitates of CrN, transforming the original martensitic phase into α-Fe (ferrite), and causing a further degradation in the corrosion resistance. © *2005 American Vacuum Society.* [DOI: 10.1116/1.1931681]

I. INTRODUCTION

Martensitic stainless steels (MSSs) are iron alloys widely used because of their unmatched properties of hardenability and wear resistance as well as corrosion resistance. However, more strident working material conditions are necessary, demanding better alloy properties. Plasma immersion ion implantation (PI^3) is a well established method for surface modification that has been successfully applied to the nitriding of austenitic stainless steel (ASS).[1,2] The high applied bias voltages and the low background partial pressure of oxygen in the process chamber are the key, controlling the formation of chromium oxides on the surface.[3–5] In fact, a richer and thicker nitrogen implanted zone can be obtained by both the energetic ion bombardment and low surface oxide formation. The combined effect augments the surface nitrogen retention, i.e., the surface nitrogen chemical potential, hence improving the diffusion process in this class of alloys.[6]

MSS are meta-stable iron alloys and as such they require careful treatment conditions to avoid undesirable phase transformation during heat treatment processes such as nitriding. These types of steels are obtained by fast cooling, inducing martensitic transformations, followed by appropriate tempering to stabilize the microstructure. As for nitriding of ASS, the main goal in nitriding of MSS is to improve the surface tribological properties while simultaneously maintaining the corrosion resistance in the modification zone. Previous authors have shown the subtle relationship among several processing parameters, such as temperature, process time, and substrate conditions.[7–10] However, many questions are still unanswered and more work is necessary to optimize the process. Moreover, due to the complexity of the metastability of MSS, some structural questions remain unresolved. For instance, what are, if any, the phase transformations involved in the nitriding process? How does the corrosion resistance degradation begin? The role of chromium nitride (CrN) precipitation is presumed to be the critical process to be avoided. Therefore, a better understanding of the physical–chemical processes leading to CrN precipitation in plasma nitriding of MSS is fundamental.

In this article we report the results of PI^3 nitriding treatments of MSS at different temperatures and processing times. The aim of the study is to investigate the physical–chemical transformations, structure, and morphology, focusing on the changes in the corrosion resistance. The article is organized as follows. In Sec. II, the experimental conditions used are introduced, stressing the techniques employed in the study. In Sec. III, the experimental results are presented, analyzed, and discussed focusing on the microscopic phenomena leading to chemical elements diffusion and CrN precipitation. Finally, in Sec. IV, the conclusions are presented.

[a)]Author to whom correspondence should be addressed; electronic mail: cafiguer@ifi.unicamp.br

TABLE I. Summary of the treatment conditions of AISI 420 by PI^3. Nitrogen gas pressure was 15 μbar, HV pulse length of 100μs, pulse duty cycle adjusted to maintain a constant dose rate.

Temperature, (°C)	Time process, (h)	HV bias voltage (keV)	Dose rate (10^{14} ions cm^{-2} s^{-1})
360	1, 4, or 9	5, 15, or 25	0.5, 1.0, or 2.5
430	1, 4, or 9	5, 15, or 25	0.5, 1.0, or 2.5
500	1, 4, or 9	5, 15, or 25	0.5, 1.0, or 2.5

II. EXPERIMENT

The study is based on martensitic stainless steel AISI 420 (C: 0.3, Si: <1.0, P: <0.04, S: <0.03, Mn: <1.0, Ni <1.0, Cr: 13.0, Fe: balance). Several disks ~25 mm diameter and ~4 mm thick were cut from bar stock and then ground and polished to a 1 μm size diamond abrasive powder finishing. Before nitrogen implantation, the samples were hardened at 1040 °C for 1 h and tempered at 530 °C for 1 h. This material tempering temperature guarantees no phase structure changes at working temperatures below 510 °C.[11] These samples were processed using the PI^3 system described elsewhere (ANSTO).[12] An array of samples implanted at each of three process temperatures, times, PI^3 bias voltages, and ion dose rates was studied. Table I shows a summary of the treatment conditions. The dependency of the resultant nitrided layers was experimentally determined to be more dominated by the variations in process temperature and time, rather than by ion energy and implantation dose. Indeed, these parameters determine the material structural modifications and corrosion behavior reported in this article.

The phase evolution was studied by x-ray diffraction (XRD) using a Siemens D500 x-ray diffractometer with a Co $K\alpha$ x-ray source in the conventional Bragg–Brentano geometry. The surface morphology of the as-nitrided layers was observed by scanning electron microscopy (SEM) using secondary electron images (SEIs) and backscattered electron images (BEIs) in a JEOL JSM-6400. Standard metallographic cross sections were prepared and etched with Marble's solution (10 g copper sulfate in 100 ml of 6 M hydrochloric acid) to reveal the microstructure of the nitrided layers. In order to determine chemical composition, samples were analyzed by energy dispersive x-rays spectroscopy (EDS) in the SEM. As complementary data, x-ray photoemission spectroscopy (XPS) measurements were also performed in ultrahigh vacuum with a VG ESCALAB 220i-XL system employing a monochromatic Al $K\alpha$ (1486.6 eV) x-ray source. The x-ray gun was operated at 120 W, and the spectrometer pass energy was set at 20 eV for regional scans. The diameter of the analysis area was approximately 500 μm, and the thickness of the probed surface layer was less than 5 nm. In order to remove the oxidized surface layer, the samples were bombarded by 5 keV Ar^+ ions ($P \sim 2.3\times10^{-7}$ mbar). The binding energies were calibrated relative to the Fermi level arbitrarily taken at 0 eV.

Finally, the corrosion behavior of the nitrided samples was studied by electrochemical methods. One cm^2 pieces of the samples were embedded in bakelite resin so that only the nitrided surface was exposed, and an insulated electrical connection made to the rear of the sample. Measurements were performed with a VoltaLab PGZ 402 using a conventional three-electrode cell. A solution of 3% NaCl was made from analytical grade reagent and de-ionized water (18.2 MΩ). The auxiliary electrode was a Pt wire and all voltages were measured against a Ag/AgCl (1 M) reference electrode. The potentiostatic anodic polarization curves were obtained at a potential scan rate of 1 mV s^{-1}.

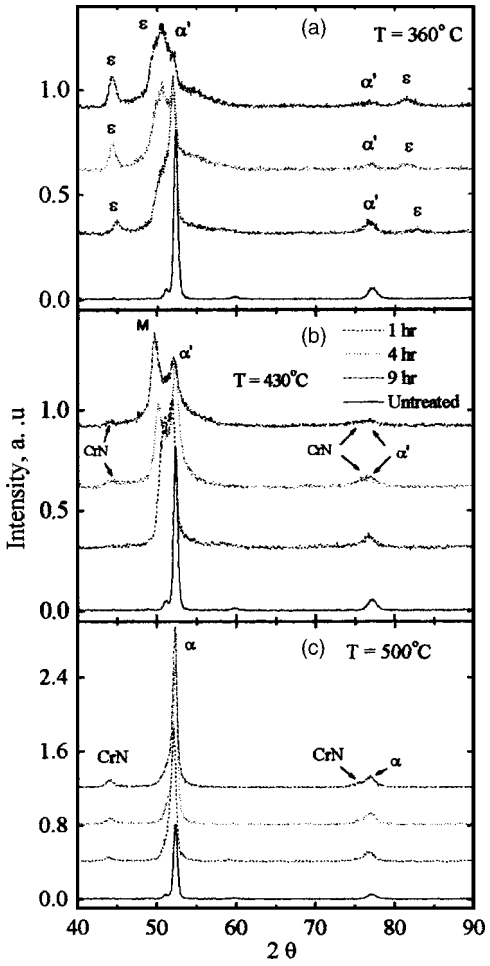

FIG. 1. Evolution of the XRD patterns with the time at constant temperature of (a) 360 °C, (b) 430 °C, and (c) 500 °C.

III. RESULTS AND DISCUSSION

In this section, we explain our results by the fact that the treatment temperature is the main parameter controlling the diffusion processes during the PI^3 nitriding of MSS. Moreover, the process temperature dependence of the diffusing elements such as nitrogen, carbon, and chromium, result in a complex phase formation.[13] On the other hand, the process time determines the proportion of the different phases formed, and the depth to which the nitrided layer extends.

At the lowest temperature, the diffusion process is weak and a surface rich nitrogen phase is formed. Figure 1(a) shows the evolution of the different phases at different treat-

TABLE II. Summary of the phases obtained by XRD.

Temperature (°C)	Phases by XRD
Untreated	$\alpha^{\ni}$, little γ
360	ε-$(Fe,Cr)_3N$, $\alpha^{\ni}$
430	$\alpha^{\ni}$, M, little CrN
500	α, CrN

ment times at 360 °C implantation temperature. For short-time implantation times, the original martensitic phase suffers a further expansion. Increasing implantation times leads to ε-$(Fe,Cr)_3N$ formation by nitrogen accumulation.

At intermediate temperatures, higher nitrogen diffusion avoids the ε-$(Fe,Cr)_3N$ phase formation (less nitrogen retention in the structure) in favor of the expansion of the original martensitic phase. Figure 1(b) shows the evolution of the original martensitic phase toward an expanded α phase and a small CrN precipitation at 430 °C as a function of implantation time.

It is important to remark that the peak at 82°, corresponding to the ε phase in Fig. 1(a), disappears at 430 °C [see Fig. 1(b)]. On the other hand, a reflection peak associated with "expanded martensite" by Kim *et al.*, clearly arises at 50° [band *M*, Fig. 1(b)]. This phase is constituted by a supersaturate compound of nitrogen in the original martensitic matrix. Indeed, this conclusion is confirmed by similar XRD patterns obtained in supersaturate compounds by Kim *et al.*[7] Moreover, it was recently reported that elements such as chromium, vanadium, and other transition metals, can stabilize the α phase. These reports showed nitrogen concentrations well above 0.1%, i.e., the maximum nitrogen solubility in the α phase, prior to its transformation into the gamma γ' phase.[14] Finally, at the highest studied temperature implantation, the increasing Cr mobility induces precipitation such as CrN from the martensitic matrix. As observed in Fig. 1(c) it shows similar behaviors in samples nitrided during different times at 500 °C, i.e., the martensitic phase is degraded to α-Fe (ferrite) and CrN. Table II shows a summary of the phases obtained at different process temperatures.

The surface and cross-section analysis by SEM and EDS of these samples support the changes in the crystalline structures presented above. Figures 2(a) and 2(b) show the SEI and BEI micrographs corresponding to a sample implanted at 360 °C during 9 h, respectively. The grain boundaries are indicated to help in the interpretation. In order to compare the chromium content in the matrix and at the grain boundary, EDS measurements were performed [Fig. 2(b)]. The backscattering photos were obtained in the composition mode where a darker tonality means a higher concentration of light elements.[15] In fact, as observed in the micrograph, grain boundary dislocations promote the accumulation of higher nitrogen concentration. A similar amount of chromium content measured in the two regions studied agrees with the XRD pattern shown in Fig. 1(a), where segregation was not observed.

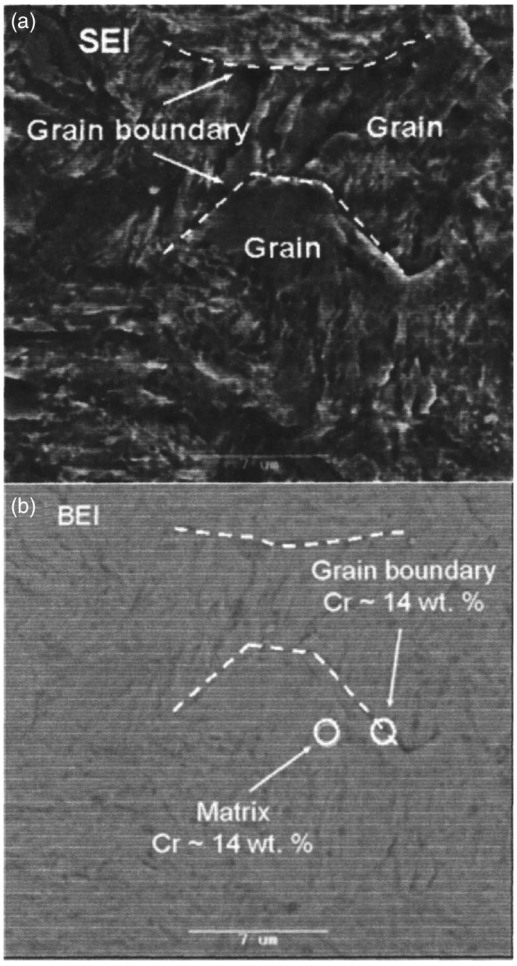

FIG. 2. (a) SEI and (b) BEI photos of the surface of a sample at 360 °C and 9 h, respectively. The EDS measurements are shown on the BEI photo. The dashed line is a guide for the eyes.

Figures 3(a) and 3(b) show the SEI and BEI micrographs corresponding to a sample implanted at 430 °C during 9 h. Figure 3(a) shows well-defined grain boundaries. In contrast, Fig. 3(b) shows dark spots distributed on the surface, preferentially at the grain boundary. In these samples, however, different chemical compositions between the matrix and the grain boundary were found. The reason for these findings relies on the fact that higher temperature treatments produce two effects. First, nitrogen diffuses faster at 430 °C than at 360 °C, enhancing the expansion of the original martensitic phase. Second, due to the temperature, Cr mobility increases, promoting grain boundary precipitations. The higher nitrogen concentration and density of dislocations located at the grain boundary act as preferential nucleating sites.[16]

Figures 4(a) and 4(b) show the SEI and BEI micrographs corresponding to a sample implanted at 500 °C during 9 h. The relatively high temperature treatment substantially augments chromium mobility, transforming the original martensitic phase to α-Fe (ferrite) and CrN. The micrographs do not reveal the grain boundaries in the material and the observed precipitates are larger and randomly distributed.

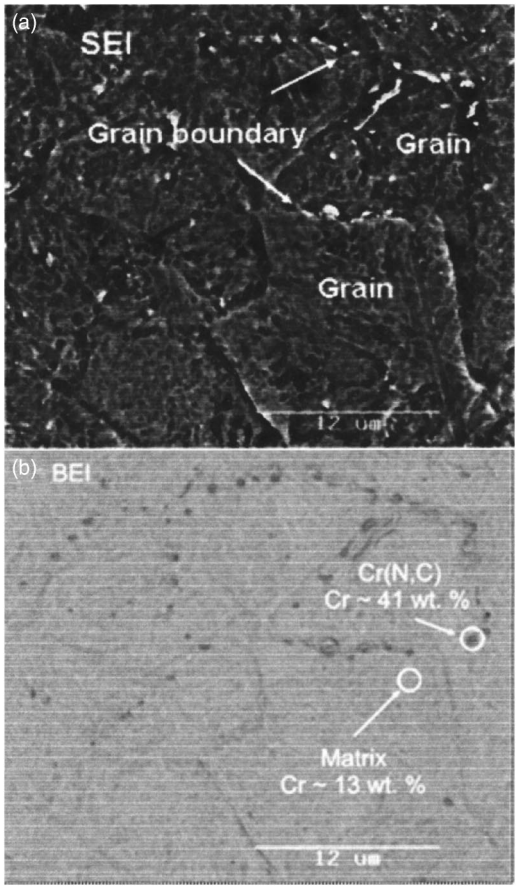

FIG. 3. SEI and BEI photos of the surface of a sample at 430 °C and 9 h, respectively. The EDS measurements are shown on the BEI photo.

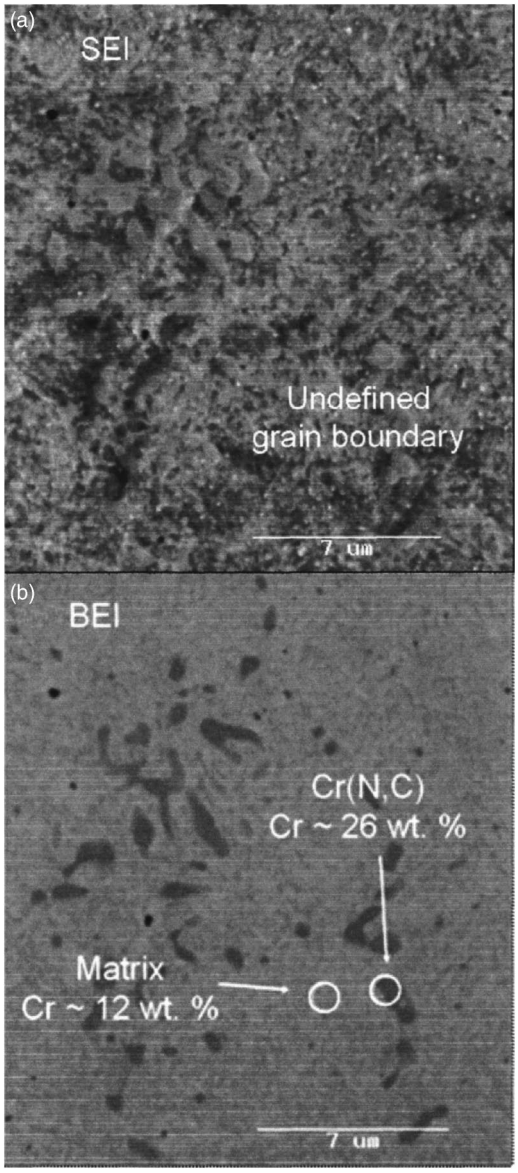

FIG. 4. SEI and BEI photos of the surface of a sample at 500 °C and 9 h, respectively. The EDS measurements are shown on the BEI photo.

The cross-section analysis of the samples reinforces these interpretations. Figures 5(a)–5(c) show the cross-section micrograph in the BEI mode of samples treated at 360 °C (9 h), 430 °C (9 h), and 500 °C (4 h), respectively. In samples treated at 360 °C during 9 h implantation, a compact nitrided layer, highly resistant to chemical etching, is formed [Fig. 5(a)]. On the other hand, the well-defined grain boundaries with CrN precipitates observed in Fig. 5(b) indicate a worse corrosion resistance of the nitrided layer. The dark zone observed at the top of the nitrided layer [Fig. 5(c)] is attributed to substantial segregations of CrN. Finally, the nitrided layer was directly evaluated from the micrographs. As expected, the nitrided thickness follows a time parabolic law (does not show).

In order to identify the precipitates shown in Fig. 3(b) and 4(b), XPS measurements were performed on the treated samples. Previously, the samples were sputtered with Ar^+. This cleaning process, however, is mandatory since the samples were exposed to the atmosphere and moisture normally adheres on the surface material. It is important to note that an oxygen atomic content, with a depth of 9%, after removing the surface contamination layer, was detected in the sample processed at 500 °C. Figures 6(a) and 6(b) show the N 1*s*, core electron level photoemission spectra of two important cases: samples implanted at 360 and 500 °C, respectively. The N 1*s* band is attributed to nitrogen forming several metallic compounds and can be identified by a deconvolution procedure.[17,18] The more probable constituents of the N 1*s* band are obtained from the previous XRD analysis, i.e., CrN, ε-$(Fe,Cr)_3N$, and α-ferrite. As noted, only N bonded to Cr, i.e., CrN, shows a marked energy shift ("chemical shifts").[19,20] On the increasing temperature, the N 1*s* core electron level shifts to lower binding energies, in agreement with the formation of CrN precipitates observed in the BEI micrograph [see Fig. 4(b)]. The oxygen effect is neglected because NO_x species were not detected and its strong electronegativity should shift the N 1*s* peak to higher binding energies, contrary to our observations.

The findings described are reflected in the corrosion behavior of the treated alloys. Figure 7 shows the anodic polarization curves of three treated samples implanted at different temperatures and a fixed time (9 h). For comparison

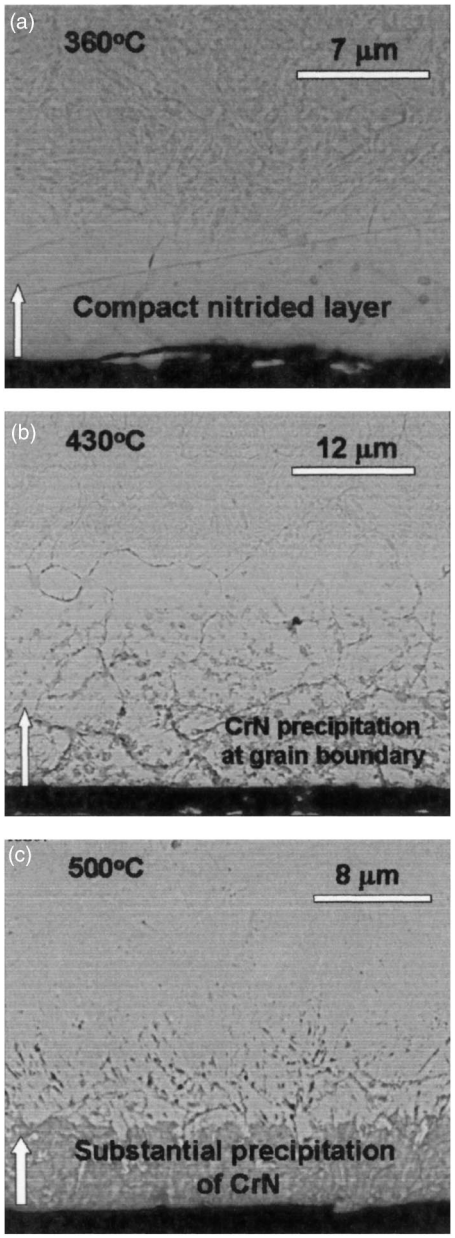

FIG. 5. (a), (b), (c) SEM photos in cross-section of treated samples at variable temperatures (indicated on the photo) in the BEI mode.

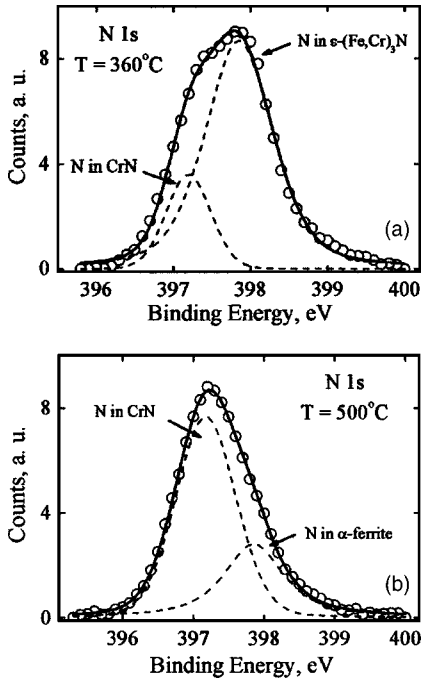

FIG. 6. N 1*s* core-level photoemission spectra of treated samples at temperatures of (a) 360 °C and (b) 500 °C, respectively. Each peak is deconvoluted in two contributions.

purposes, a curve corresponding to the untreated material is also included. As observed, all curves have a passivating zone (low current density) before reaching the breakdown potential, i.e., where the metal species dissolution from the sample electrode starts. A shift to more positive potential indicates a higher level of corrosion resistance. Table III shows the breakdown potential of these analyzed samples. Bearing in mind that the corrosion properties are determined by the hostile surrounding medium, the presence of chloride ions probes the pitting corrosion, i.e., the possible penetration path of the aggressive ions.[21] The following behavior is observed in the potentiodynamic curves. First, for lower implantation temperature, the curve shifts to higher values, indicating a better pitting corrosion resistance. Second, the current density of samples treated at 360 °C is the lowest one, even when compared to the untreated material. Therefore, one can conclude that the CrN precipitates reduce the corrosion resistance by intergranular sensitization.[22] The apparently similar corrosion behavior of the sample implanted at 430 °C, with the untreated one, is a mixture of two mechanisms where chemically the matrix shows an excellent corrosion resistance (even compared to the untreated sample) in contrast to a poor resistance at the grain boundary. Finally, the formation of a more compact structure, i.e., the ε-$(Fe,Cr)_3N$ phase without any chromium segregation, improves the corrosion resistance of the original material as well as tribological properties like hardness and wear resistance.

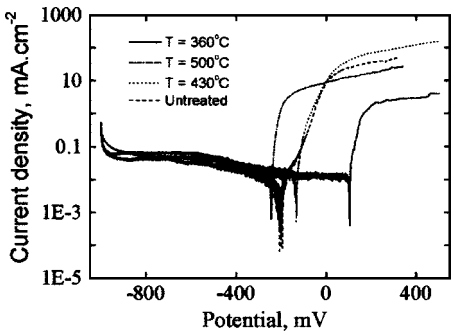

FIG. 7. Anodic polarization curves obtained in 3% NaCl solution for treated samples at variable temperatures and fixed time process of 9 h.

TABLE III. Breakdown potentials obtained by potentiostatic anodic polarization in 3% NaCl of treated samples at variable temperature and fixed time process of 9 h. The potential was corrected taking the value of the reference electrode (235 mV).

Temperature (°C)	Breakdown potential (mV)
360	104
430	−132
500	−245
Untreated	−200

IV. CONCLUSION

Martensitic stainless steel AISI 420 was nitrided by the PI^3 technique at three characteristic temperatures bearing in mind industrial applications. At the lower studied implantation temperature ($\sim$360 °C), a compact layer of ε-$(Fe,Cr)_3N$ is formed, preserving the material grain morphology. The sample pitting corrosion resistance is considerably improved when compared to untreated material. At intermediate implantation temperatures ($\sim$430 °C), a structure akin to "expanded martensite" is obtained. This treatment condition induces morphology changes and CrN precipitates, mostly at the grain boundary, diminishing the material resistance to pitting corrosion. Finally, at higher temperatures ($\sim$500 °C), the original martensitic phase transforms to α-Fe (ferrite) and further precipitation of CrN. These effects are a consequence of the relatively high Cr mobility at this temperature. Therefore, the material morphology is surprisingly different as compared to the one obtained at lower implantation temperature. Moreover, in the case of the material treated at the highest temperature studied, the grain boundaries are hardly distinguished and CrN random precipitates are presented. Consequently, a much worse result of pitting corrosion resistance is obtained.

ACKNOWLEDGMENTS

The authors are indebted to FAPESP and ANSTO for supporting CAF to develop Project No. 00/09334-9 at ANSTO. One of the authors (F.A.) is a CNPq fellow. C.A.F. is a Fapesp fellow. The authors thank V. Luca fundamentally for his friendship and for equipment facilities and Y. Whiteley for her English lessons, and J. Bowdler and H. Li for sample preparations and SEM advice, respectively.

[1]G. A. Collins, R. Hutchings, K. T. Short, and J. Tendys, Heat Treat. Met. **4**, 91 (1995).
[2]G. A. Collins, R. Hutchings, K. T. Short, J. Tendys, and C. H. VanDerValk, Surf. Coat. Technol. **84**, 537 (1996).
[3]J. M. Priest, M. J. Baldwin, M. P. Fewell, S. C. Haydon, G. A. Collins, K. T. Short, and J. Tendys, Thin Solid Films **345**, 113 (1999).
[4]C. A. Figueroa, D. Wisnivesky, and F. Alvarez, J. Appl. Phys. **92**, 764 (2002).
[5]C. A. Figueroa, A. S Ferlauto, and F. Alvarez, J. Appl. Phys. **94**, 5435 (2003).
[6]C. A. Figueroa and F. Alvarez (unpublished).
[7]S. K. Kim, J. S. Yoo, J. M. Priest, and M. P Fewell, Surf. Coat. Technol. **163–164**, 380 (2003).
[8]P. Corengia, G. Ybarra, C. Moina, A. Cabo, and E. Broitman, Surf. Coat. Technol. (in press).
[9]I. Alphonsa, A. Chainani, P. M. Raole, B. Ganguli, and P. I. John, Surf. Coat. Technol. **150**, 263 (2002).
[10]A. Leyland, D. B. Lewis, P. R. Stevenson, and A. Matthews, Surf. Coat. Technol. **62**, 608 (1993).
[11]R. W. K. Honeycombe and H. K. D. H. Bhadeshia, *Steels: Microstructure and Properties*, 2nd ed. (Edward Arnold, London, 1995), p. 171.
[12]G. A. Collins, R. Hutchings, K. T. Short, and J. Tendys, Surf. Coat. Technol. **103–104**, 212 (1998).
[13]D. E. Jiang and E. A. Carter, Phys. Rev. B **67**, 214103 (2003).
[14]A. Muñoz-Páez, J. I. F. Peruchena, J. P. Espinós, A. Justo, F. Castañeda, S. Días-Moreno, and D. T. Bowron, Chem. Mater. **14**, 3220 (2002).
[15]L. Reimer, *Scanning Electron Microscopy: Physics of Image Formation and Microanalysis* (Springer, Berlin, 1985).
[16]*Proceedings Symposium of TMS-AIME Heat Treatment Committee, TMS Fall Meeting*, Niagara Falls, New York, 1976, edited by K. C. Russell and H. I. Aaronson (The Metallurgical Society of AIME, 1976).
[17]E. J. Miola, S. D. de Souza, P. A. P. Nascente, M. Olzon-Dionysio, C. A. Olivieri, and D. Spinelli, Appl. Surf. Sci. **144–145**, 272 (1999).
[18]J. P. Riviere, M. Cahoreau, and P. Meheust, J. Appl. Phys. **91**, 6361 (2002).
[19]O. Nishimura, K. Yabe, and M. Iwaki, J. Electron Spectrosc. Relat. Phenom. **49**, 335 (1989).
[20]H. Tsujimura, T. Goto, and Y. Ito, Mater. Sci. Eng., A **355**, 315 (2003).
[21]C. Blawert, H. Kalvelage, B. L. Mordike, G. A. Collins, K. T. Short, Y. Jirásková, and O. Schneeweiss, Surf. Coat. Technol. **136**, 181 (2001).
[22]M. Samandi, B. A. Shedden, D. I. Smith, G. A. Collins, R. Hutchins, and S. Tendys, Surf. Coat. Technol. **59**, 261 (1993).